nature communications

Article

https://doi.org/10.1038/s41467-025-58337-w

Covalent organic framework without cocatalyst loading for efficient photocatalytic sacrificial hydrogen production from water

Received: 26 February 2024

Accepted: 19 March 2025

Published online: 28 March 2025

Check for updates

Xuejiao Du[1,3], Haifeng Ji[1,3], Yang Xu[1], Shiwen Du[2], Zhaochi Feng[2], Beibei Dong[1] ✉, Ruihu Wang[1] ✉ & Fuxiang Zhang[2] ✉

Metals are typically essential as either integral components within photocatalysts or as cocatalyst modifiers to enable efficient artificial photosynthesis, such as water splitting and carbon dioxide reduction. However, developing photocatalysts that function effectively without metal cocatalysts remains challenging due to their cost and scarcity. Here we show a nonstoichiometric β-ketoenamine-linked covalent organic framework that operates without cocatalysts, achieving hydrogen production rates of 15.48 mmol·g^{-1}·h^{-1} from seawater and 22.45 mmol·g^{-1}·h^{-1} from water with an ascorbic acid scavenger under visible light. It outperforms many reported platinum-modified covalent organic frameworks and metal-containing inorganic photocatalysts. The enhanced performance is attributed to its broad light absorption edge extending to approximately 660 nm, efficient charge separation, and the presence of abundant active oxygen sites derived from carbonyl groups, which exhibit a low hydrogen-binding Gibbs free energy change. This work lays the groundwork for designing cost-effective photocatalytic systems suitable for large-scale hydrogen production.

Achieving efficient solar-to-chemical conversion, such as photocatalytic water splitting and carbon dioxide reduction[1–4], relies heavily on semiconductors capable of broad visible light utilisation. To this end, extensive research has focused on metal-containing inorganic semiconductors[5–7] (e.g., metal oxides, (oxy)nitrides, (oxy)halides, and (oxy)sulfides) and organic-inorganic hybrid materials[8,9] like metal-organic frameworks (MOFs). A common feature of these materials is the incorporation of metals within their crystalline structures, with noble metals such as platinum often used as cocatalyst modifiers to enhance activity by providing active sites. To circumvent the reliance on metals, metal-free organic semiconductors, including carbon nitride[10] and covalent organic frameworks (COFs)[11,12], have been explored. However, many organic polymers and COFs lack intrinsic activity for water splitting or carbon dioxide reduction, necessitating the use of (noble) metal-based cocatalysts to improve photocatalytic reaction kinetics[13,14]. This dependence on metals, particularly noble ones, significantly increases costs and limits scalability due to their scarcity.

A major limitation of metal-based cocatalysts is the energy loss at the photocatalyst-cocatalyst interface, caused by lattice or energy mismatches[15]. This mismatch hinders interfacial charge separation, a critical factor for solar-to-chemical conversion efficiency[16]. Despite extensive efforts to improve interfacial charge separation[17,18], effective solutions remain limited. An alternative approach is to eliminate

[1]School of Chemical Engineering and Technology, Yanzhao Green Chemical Engineering Laboratory, Hebei University of Technology, Tianjin, China. [2]Dalian Institute of Chemical Physics, Chinese Academy of Sciences, Dalian, China. [3]These authors contributed equally: Xuejiao Du, Haifeng Ji.
✉e-mail: bbdong@hebut.edu.cn; ruihu@hebut.edu.cn; fxzhang@dicp.ac.cn

cocatalysts entirely, requiring the photocatalyst itself to incorporate effective catalytic active sites. While progress has been made by embedding metal-coordinated catalytic structures into MOFs or COFs for hydrogen production[9,19], developing a photocatalyst that achieves efficient water splitting without metal-based cocatalysts remains a significant challenge.

In this study, we present a nonstoichiometric β-ketoenamine-linked Tp-Py-COF that serves as an efficient photocatalyst without the need for additional cocatalysts, achieving effective sacrificial hydrogen production from both water and seawater. Its hydrogen evolution rate surpasses many reported platinum-modified COFs, metal-containing inorganic photocatalysts, and their composites. While metal-based cocatalysts have been widely used to enhance photocatalytic materials, this work demonstrates that cocatalyst modification is not necessary for achieving high activity. Notably, the abundant carbonyl groups (C = O) within the structure are identified as active sites for proton reduction, exhibiting a relatively low hydrogen-binding free energy change (ΔG). The efficient photocatalytic water splitting performance is attributed to its structural advantages, including broad visible light absorption, embedded highly active proton reduction sites, and the absence of cocatalysts, which collectively enhance key processes such as light absorption, surface catalysis, and charge separation.

Results

Preparation and characterizations of Tp-Py-COF

Tp-Py-COF was synthesised through a Schiff base reaction between 1,3,5-triformylphloroglucinol (Tp) and 1,3,6,8-tetrakis(4-aminophenyl) pyrene (Py), catalysed by acetic acid in a mesitylene/1,4-dioxane solvent mixture (7:3 volume ratio) at 120 °C for three days (Fig. 1a). The crystallinity of the material depends on the molar ratio of Tp to Py monomers, with an optimal ratio of 4:3 yielding the best crystallisation (Supplementary Fig. S1). Unless otherwise specified, the Tp-Py-COF synthesised at this ratio was used for all activity tests and characterisation in this study. The crystalline structure, illustrated in Fig. 1b, was confirmed experimentally by powder X-ray diffraction (PXRD, Fig. 1c), showing excellent agreement (R_{wp} = 6.56%, R_p = 5.11%) with the simulated AA stacking model in the triclinic P1 space group (Supplementary Table S1).

The chemical structure of Tp-Py-COF, identified as a β-ketoenamine-linked framework, was verified using Fourier transform infrared (FTIR) spectroscopy, solid-state ^{13}C nuclear magnetic resonance (^{13}C NMR), and X-ray photoelectron spectroscopy (XPS). In the FTIR spectra (Fig. 2a), the characteristic peaks for -NH_2 (3214 and 3347 cm^{-1}) in Py and -CH=O (1646 cm^{-1}) in Tp significantly decreased, while new peaks corresponding to C=C (1578 cm^{-1}) in the (C=C)-N unit and C-N (1293 cm^{-1}) in the C-NH linkage emerged[20,21]. Further evidence was provided by the ^{13}C NMR resonance at 147 ppm (Fig. 2b)[22] and the N *1 s* XPS signal at 400.0 eV (Fig. 2c)[23], both attributed to the C-N bond in the β-ketoenamine linkage. Additionally, residual aldehyde groups were detected, as indicated by the FTIR peak at 1663 cm^{-1} and the ^{13}C NMR resonance at 185 ppm (Fig. 2b and Supplementary Fig. S2).

Additionally, the Tp-Py-COF powder exhibits a substantial Brunauer-Emmett-Teller (BET) surface area of 658 $m^2 \cdot g^{-1}$ (Fig. 2d) and demonstrates good thermal stability up to 400 °C under a nitrogen atmosphere, as confirmed by thermogravimetric analysis (Supplementary Fig. S3a). The material displays a ribbon-like morphology, as revealed by its typical scanning and transmission electron microscope (SEM/TEM) images (Fig. 2e–f). Moreover, Fig. 2f highlights a lattice fringe of 1.47 nm, consistent with the lattice spacing of the (100) crystal plane. This alignment is supported by the prominent peak at 2θ = 6.5° in both simulated and experimental PXRD patterns, further validating the accuracy of the simulated structural model.

The Tp-Py-COF exhibits a salmon-red colour (inset of Fig. 3a) and demonstrates a broad visible light absorption edge extending to approximately 660 nm, as revealed by ultraviolet-visible diffuse reflectance spectroscopy (UV-vis DRS, Fig. 3a). This corresponds to a theoretical solar-to-hydrogen efficiency exceeding 20%. Based on the Tauc plot (inset of Fig. 3a), its direct optical bandgap energy (E_g) is calculated to be 1.88 eV. The Mott-Schottky analysis, with its positive slope, confirms the n-type semiconductor nature of Tp-Py-COF (Fig. 3b), and the flat-band potential is determined to be approximately -0.2 V (vs. RHE). Considering the typical 0.2 V positive shift of the flat-band potential relative to the conduction band position (E_{CB}) in

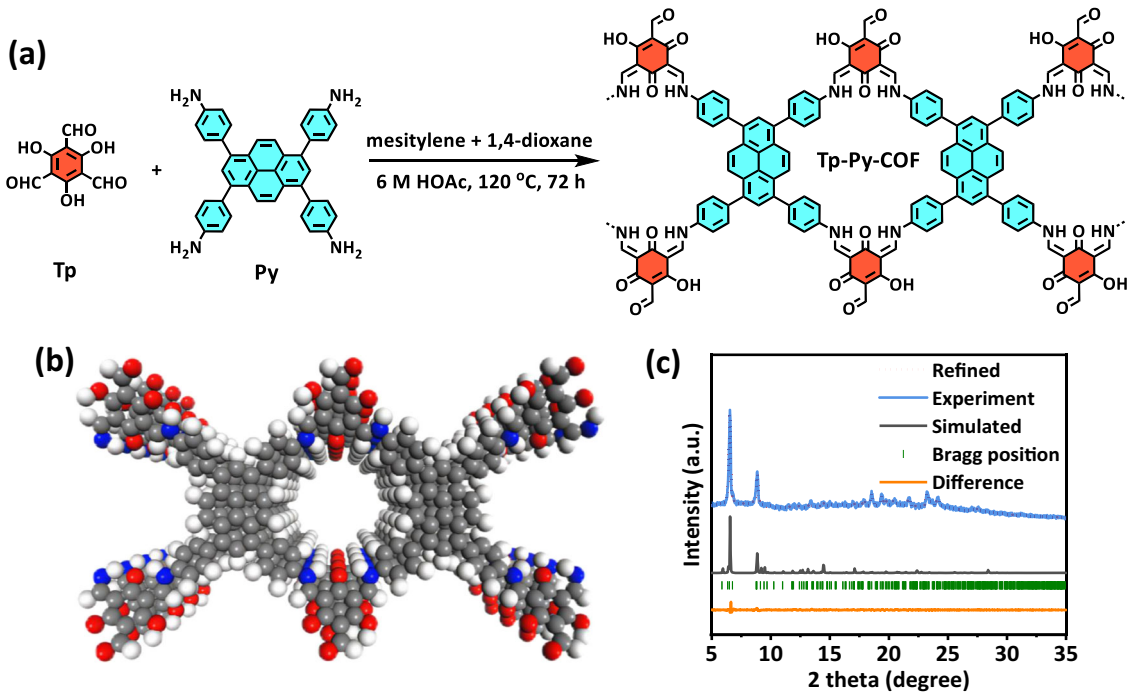

Fig. 1 | Synthesis and structural simulation of Tp-Py-COF. Schematic illustration for synthesizing Tp-Py-COF (**a**), top view (**b**), and experimental PXRD (**c**) of Tp-Py-COF. Grey, blue, red, and white atoms represent carbon, nitrogen, oxygen, and hydrogen elements, respectively. Source data are provided as a Source Data file.

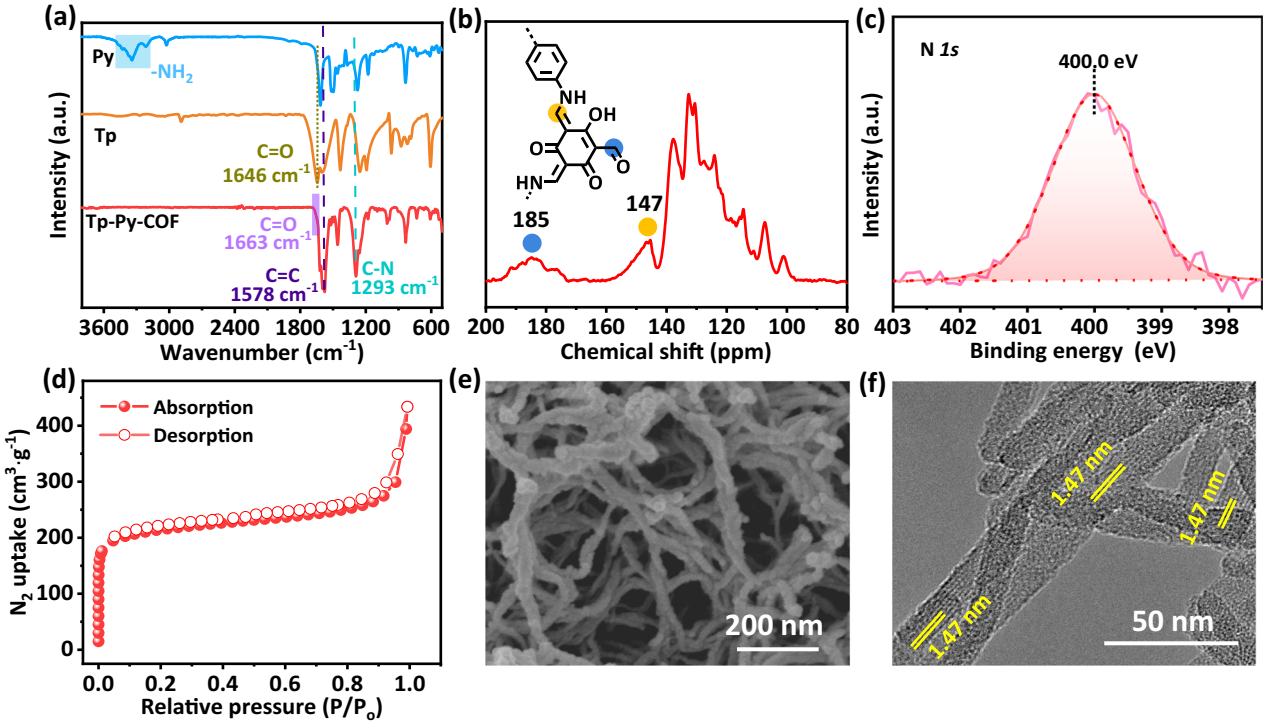

Fig. 2 | Material characterizations of Tp-Py-COF. FTIR spectra of Tp, Py, and Tp-Py-COF (**a**), ^{13}C NMR spectroscopy (**b**), N *1 s* XPS spectrum (**c**), N_2 adsorption-desorption isotherm (**d**), SEM image (**e**), and TEM image (**f**). Source data are provided as a Source Data file.

n-type semiconductors[24], the E_{CB} is estimated at -0.4 V (vs. RHE), while the valence band position (E_{VB}) is deduced to be 1.48 V (vs. RHE). These band positions confirm that Tp-Py-COF is thermodynamically capable of facilitating water splitting.

Photocatalytic measurements of Tp-Py-COF

Motivated by its promising optical and electronic properties, as well as thermodynamic feasibility, Tp-Py-COF was employed as a heterogeneous photocatalyst for visible-light-driven water splitting without the need for modifiers or cocatalysts, using ascorbic acid as a sacrificial hole scavenger (Supplementary Fig. S3b). The optimal mass-dependent yield was achieved using 2 mg of catalyst (Supplementary Fig. S3c), with hydrogen yields of 22.45 mmol·g^{-1}·h^{-1} from pure water and 15.48 mmol·g^{-1}·h^{-1} from natural seawater, outperforming many reported platinum-modified COF-based photocatalysts (Supplementary Table S2) and metal-containing inorganic photocatalysts, including their composites (Supplementary Table S3). Wavelength-dependent experiments revealed that the photocatalytic activity of Tp-Py-COF aligns with its UV-vis DRS profile, with hydrogen evolution even observed under 600 nm irradiation (Fig. 3c), highlighting its efficiency. The apparent quantum efficiency for hydrogen evolution at 420 nm was measured at 3.3%. Long-term stability tests over 20 h (four cycles, Fig. 3d) showed no significant degradation, and the PXRD and FTIR spectra of Tp-Py-COF remained consistent before and after the reaction (Supplementary Fig. S4a, b). Notably, no detectable Cl_2 or ClO^- was found in the seawater reaction solution, indicating that chloride ions were not oxidised by photogenerated holes. The negative zeta potential of Tp-Py-COF in seawater (Supplementary Fig. S4c) suggests that chloride ions are repelled from the catalyst surface due to electrostatic effects. Additionally, calculations of chloride ion adsorption ΔG confirm that chloride ions are not preferentially adsorbed on the catalyst surface (Supplementary Fig. S4d), explaining the comparable photocatalytic performance in seawater and freshwater.

Notably, no N_2 evolution was observed during prolonged irradiation, suggesting strong nitrogen binding within the Tp-Py-COF structure. Over 20 h, the total hydrogen evolved reached approximately 313 mmol·g^{-1}, confirming that water, rather than COF decomposition, was the primary hydrogen source. These findings highlight the stability of the photocatalyst for sustained sacrificial hydrogen production from water. Significantly, a Tp-Py-COF thin film (9.6 cm^2) consistently generated visible H_2 bubbles under visible light irradiation (Supplementary Video S1), demonstrating its potential for scalable solar-driven hydrogen production. Furthermore, inductively coupled plasma, XPS, and elemental mapping analyses confirmed the absence of Pd or Pt metals in Tp-Py-COF, or their presence below the detection limits of these techniques (Supplementary Fig. S5 and S6). Importantly, the addition of noble metals, even at optimal levels, did not enhance the photocatalytic hydrogen evolution rate (Supplementary Fig. S7), reinforcing that the COF itself, without cocatalysts, is capable of efficiently driving surface catalysis for sacrificial hydrogen production from water.

Unravelling reaction mechanisms and charge separation dynamics

To understand the efficient hydrogen evolution of Tp-Py-COF without metals or cocatalysts, density functional theory (DFT) calculations were conducted to identify the catalytic active sites for proton reduction. Various potential structural sites of Tp-Py-COF were examined, as detailed in Supplementary Fig. S8. As shown in Fig. 4a, the oxygen atoms (O1) on the carbonyl groups (C=O) exhibit the lowest hydrogen-binding ΔG of -0.09 eV, indicating that these sites are favourable for proton adsorption and reduction into hydrogen[25]. This suggests that the abundant O1 sites on the carbonyl groups act as the primary active centres for proton reduction during photocatalytic hydrogen production. To further validate this, in situ FTIR spectroscopy was used to monitor key intermediate species. The intensity of the C=O peaks decreased, while the C-O peaks increased over prolonged illumination (Supplementary Fig. S9), further inferring that proton reduction occurs predominantly at the oxygen sites of the carbonyl groups.

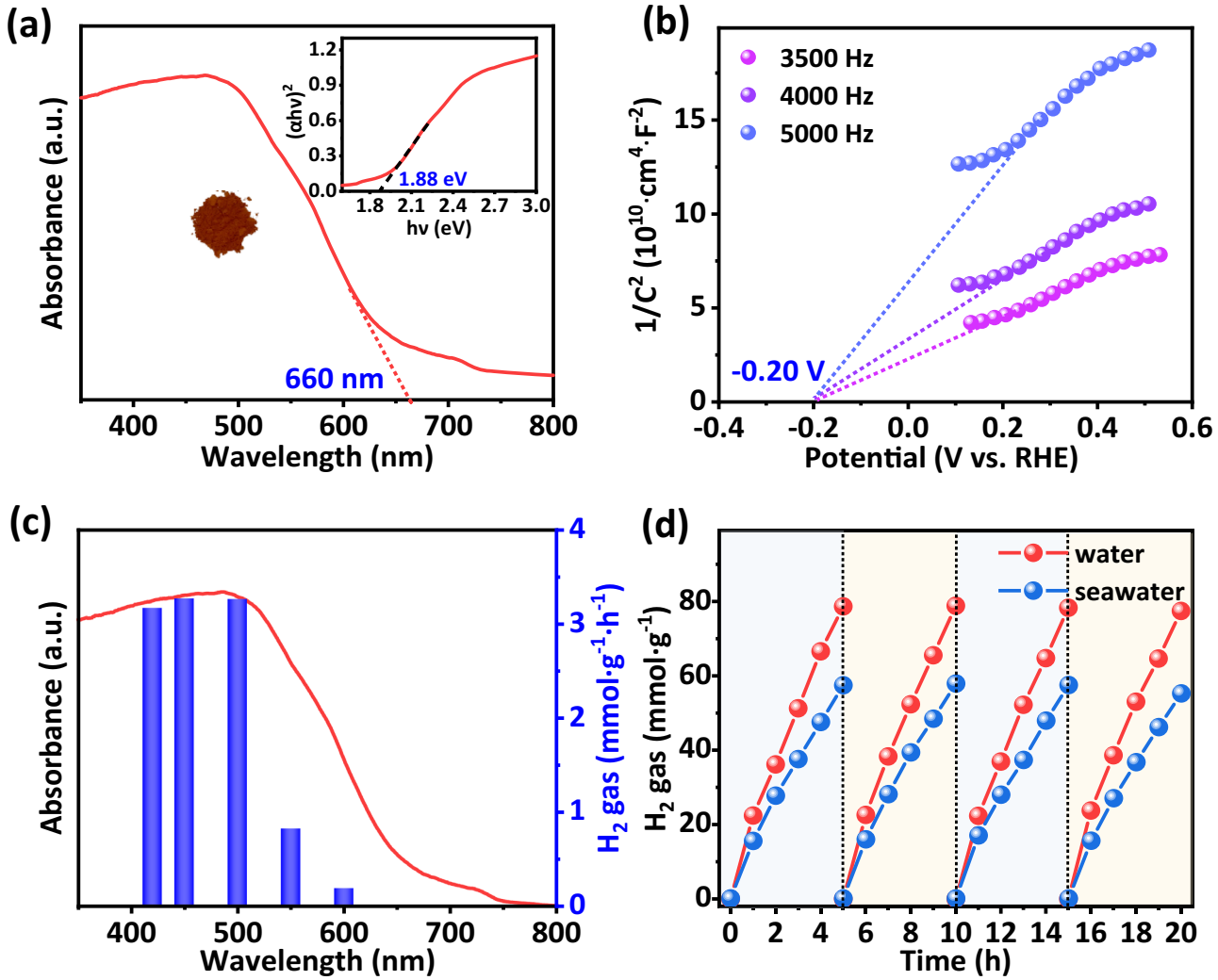

Fig. 3 | Optic and electronic properties and photocatalytic performances of Tp-Py-COF under visible light irradiation. UV–vis DRS and Tauc plot (inset) (**a**), Mott –Schottky curves (**b**), wavelength-dependent hydrogen production activities from water (**c**), and hydrogen production proceeded for 20 h with intermittent evacuation every 5 h (**d**). Reaction condition: 2 mg catalyst, 100 mL water or seawater containing 0.1 M ascorbic acid, λ ≥ 420 nm, and i = 20 A). Source data are provided as a Source Data file.

To clarify the role of O1 sites in carbonyl groups for photocatalytic hydrogen production in Tp-Py-COF, three control samples—TFB-Py-COF, HTA-Py-COF, and DHTA-Py-COF—were synthesised by substituting Tp with 1,3,5-triformylbenzene (TFB), 2-hydroxybenzene-1,3,5-triaformaldehyde (HTA), and 2,4-dihydroxybenzene-1,3,5-triaformaldehyde (DHTA), respectively. These samples share similar physical and photochemical properties with Tp-Py-COF and demonstrate thermodynamic feasibility for proton reduction (Supplementary Fig. S10–S14 and Table S4–S6). However, unlike Tp-Py-COF, none of the control samples exhibited detectable hydrogen production or significant photocatalytic activity under the same experimental conditions. Their performance was markedly inferior to that of Tp-Py-COF, which possesses the highest number of carbonyl groups, further supporting the proposed mechanism. Additional DFT calculations were performed to identify the factors contributing to the enhanced hydrogen evolution activity of Tp-Py-COF. The results revealed that the free hydroxyl groups in Tp-Py-COF lower the energy barrier for proton reduction at the oxygen-active sites of carbonyl groups (Supplementary Fig. S15) and enhance hydrophilicity (Supplementary Fig. S16). These findings explain why Tp-Py-COF outperforms the other materials in the series.

The charge carrier dynamics of Tp-Py-COF were investigated using photoluminescence (PL) spectroscopy, photoelectrochemical current measurements, and electrochemical impedance spectroscopy (EIS). Temperature-dependent PL spectra revealed that Tp-Py-COF has a lower exciton binding energy (E_b = 18 meV) compared to the three control samples, indicating superior charge separation capability, a critical factor for photocatalytic efficiency (Supplementary Fig. S17). DFT calculations (Supplementary Fig. S18) further showed that Tp-Py-COF exhibits a higher dipole moment and stronger polarization than the control samples, explaining its enhanced charge separation observed in Fig. S17. Given that charge separation is widely regarded as the rate-determining step in photocatalytic water splitting, this improved charge separation likely underpins the high photocatalytic performance of Tp-Py-COF. Time-resolved PL spectra, which reflect radiative electron-hole recombination, demonstrated a long lifetime (0.7 ns) for Tp-Py-COF, further confirming its efficient charge separation (Supplementary Fig. S19a). Additionally, Tp-Py-COF exhibited the highest photocurrent and the smallest semicircle diameter in EIS measurements, consistent with its superior charge separation and transfer properties (Supplementary Fig. S19b,c). The electron-state density distribution of Tp-Py-COF (Fig. 4b-c) revealed that the highest

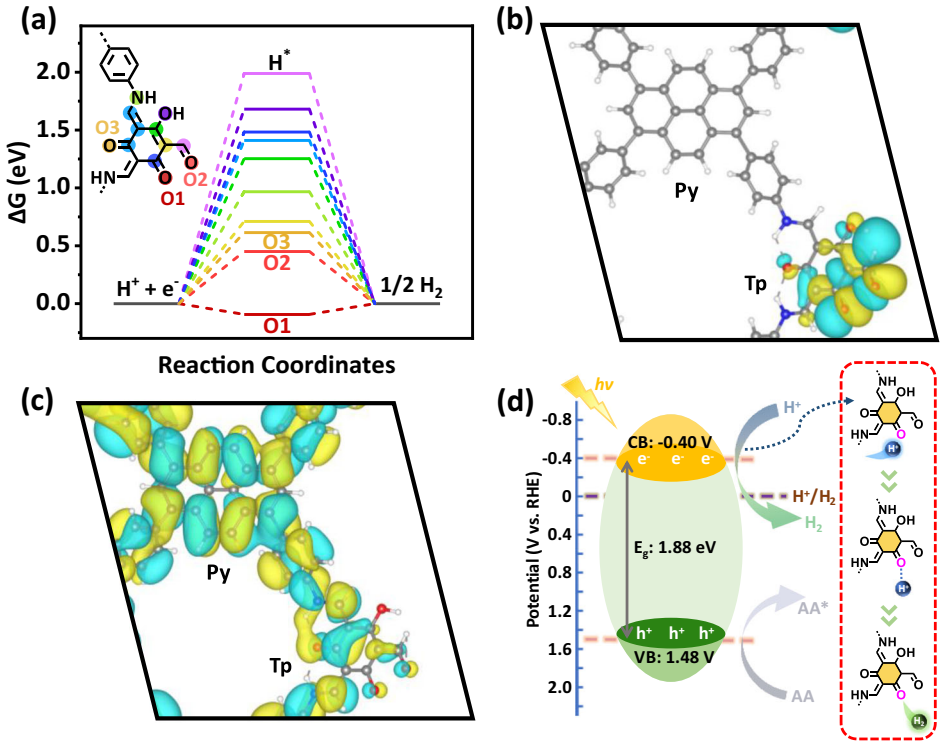

Fig. 4 | DFT calculation and mechanism study. DFT-calculated hydrogen-binding ΔG on the Tp-Py-COF model (**a**), HOMO (**b**) and LUMO (**c**) energy levels, and proposed photocatalytic mechanism (**d**). Grey, blue, red, and white atoms represent carbon, nitrogen, oxygen, and hydrogen elements, respectively.

occupied molecular orbital (HOMO) is primarily localised on part of the Tp unit, while the lowest unoccupied molecular orbital (LUMO) is distributed across both the Py unit and another part of the Tp unit. This spatial separation of HOMO and LUMO facilitates efficient charge carrier transfer, contributing to the high charge separation efficiency of Tp-Py-COF.

Based on these findings, a mechanism for photocatalytic sacrificial hydrogen production on Tp-Py-COF can be proposed (Fig. 4d). Under light irradiation, photogenerated electrons are excited from the HOMO of partial Tp units to the LUMO, where they are rapidly transferred and accumulated at the oxygen atoms of the carbonyl groups (C=O). These sites facilitate the efficient reduction of protons to hydrogen. Meanwhile, the photogenerated holes are neutralised by ascorbic acid during the oxidation process, ensuring simultaneous consumption of electrons and holes. This charge balance enables the photocatalyst to sustain continuous hydrogen production.

Discussion

In summary, we developed a nonstoichiometric n-type Tp-Py-COF semiconductor photocatalyst capable of efficient photocatalytic sacrificial hydrogen production from water under visible light irradiation. This represents a rare example of a COF-based photocatalyst achieving high hydrogen evolution performance without the need for metal or cocatalyst modification. Its superior activity and durability stand out among current studies on COF-based, metal-embedded inorganic photocatalysts, and their composites. Mechanistic insights reveal that the residual free carbonyl and hydroxyl groups in the Tp-Py-COF framework modulate its electronic structure, with specific carbonyl oxygen atoms serving as highly effective proton reduction sites. These advantageous properties—broad visible light absorption, efficient charge separation, and abundant catalytic active sites—make Tp-Py-COF a promising candidate for solar-to-chemical conversion systems. This study paves the way for developing cost-effective photocatalysts without cocatalysts, enabling scalable solar energy conversion and storage.

Methods

Synthesis of Tp-Py-COF

A mixture of 1,3,5-triformylphloroglucinol (Tp, 0.2 mmol, 42.0 mg), 1,3,6,8-tetrakis(4-aminophenyl)pyrene (Py, 0.15 mmol, 85.0 mg), mesitylene (7.0 mL), 1,4-dioxane (3.0 mL), and 6 M acetic acid (1.0 mL) was sonicated for 30 min in a reaction tube and then heated at 120 °C for 3 days. The resulting solid was collected, washed three times with methanol, tetrahydrofuran, and dichloromethane, and dried at 70 °C overnight to yield Tp-Py-COF as a red powder (80% yield). TFB-Py-COF, HTA-Py-COF, and DHTA-Py-COF were synthesised using the same procedure, with Tp replaced by 1,3,5-triformylbenzene (TFB, 0.2 mmol, 32.4 mg), 2-hydroxybenzene-1,3,5-triaformaldehyde (HTA, 0.2 mmol, 35.6 mg), and 2,4-dihydroxybenzene-1,3,5-triaformaldehyde (DHTA, 0.2 mmol, 38.8 mg), respectively.

Photocatalytic reaction

The photocatalytic reactions were conducted in a gas-closed circulation system with a top radiation reaction vessel (Labsolar-6A, Beijing Perfectlight Technology Co., Ltd.). A 300 W Xe lamp (CEL-HXF300H5, Beijing Zhongjiao Jinyuan Technology Co., Ltd.) was used to illuminate the reaction system (i = 20 A, λ ≥ 420 nm), and online GC-2014 gas chromatography (Shimadzu Corporation) was employed to analyze the evolved gases. Typically, 2 mg Tp-Py-COF or other photocatalyst was added into 100 mL water or seawater, which was sonicated and evacuated for 20 min to remove gases before irradiation. Ascorbic acid (0.1 M) was used as a hole sacrifice agent. The AQE measurement was carried out as the above mentioned condition except that a 420 nm band-pass filter was employed. The following Eq. (1) was adopted to calculate the AQE (φ):

$$\varphi\,(\%) = AR/I \times 100 \tag{1}$$

A, R, and I represent the coefficient (2 for H_2 evolution reaction), the gas evolution in an hour, and the number of incident photons in the photocatalytic system, respectively.

The photocatalytic video was recorded via irradiating the photocatalyst film, which was prepared via a simple suction filtration process, under the same condition as the above-mentioned condition. Typically, 2 mg Tp-Py-COF was dispersed in an ethanol/water mixture (volume ratio = 1:1, 20 mL) containing 0.2 mg polyvinylidene difluoride and sonicated for 2 h, which was filtrated on a microporous filter membrane and then dried in an oven at 70 °C.

(Photo)electrocatalytic test

1 mg·mL^{-1} Tp-Py-COF or other photocatalyst suspension solution in an ethanol/water mixture (volume ratio = 1:1, 2 mL) with a few droplets of 5 wt% Nafion solution were drop-casted on the working electrode of fluorine-doped tin oxide (FTO, 1 × 2.5 cm^2) conductive glass and then dried in air. Photoelectrocatalytic tests were conducted by a CHI 760E electrochemical workstation equipped with a three-electrode setup (platinum, saturated calomel, and working electrodes) in an electrolyte of 0.2 M sodium sulfate aqueous solution under visible light illumination (i = 20 A, λ ≥ 420 nm). Mott-Schottky test was carried out at an alternating current amplitude of 5 mV. Electrochemical impedance spectroscopy measurements were performed with an alternating current amplitude of 5 mV and a frequency range of 0.1 ~ 100,000 Hz.

Structural simulations

The structural models of Tp-Py-COF and other photocatalyst were generated using the Materials Studio 7.0. The lattice parameters were optimized iteratively using the Pawley refinement method until the R-weighted pattern (R_{wp}) and R-pattern (R_p) values converged and the superposition of the refined profiles showed good agreement. Atomic positions and total energies were fully optimized using the Forcite module of Materials Studio.

DFT calculations

DFT calculation was performed using the Vienna Ab initio Simulation Package[26,27]. Blöchl's all-electron-like projector augmented wave method was selected to deal with the interaction between ion cores and valence electrons. The exchange and correlation energy terms were calculated using PBE-D3 generalized gradient approximation. The kinetic plane-wave cut-off energy is set as 400 eV. The Monkhorst-Pack scheme k-points mesh was set as 2 × 2 × 1 in the structural optimization, while 9 × 9 × 1 is chosen to calculate the electronic property, with an energy convergence criterion of 1 × 10^{-5} eV. The vacuum space along the c-axis was 15 Å to eliminate spurious interaction of neighbouring layers. Under standard conditions, the Gibbs free energy of adsorbed reactive intermediate is defined as the following Eq. (2):

$$\Delta G = \Delta E_{DFT} + \Delta E_{ZPE} - T\Delta S \quad (2)$$

where ΔE_{DFT} is the reaction energy obtained from DFT calculation, ΔE_{ZPE} represents the change of zero-point energy in the reaction, T is set as 298.15 K, and ΔS indicates the entropy change of the reaction. In addition, the ΔG of each basic step is calculated using the calculated hydrogen electrode model, and the reaction steps of the hydrogen evolution reaction follow two-electron transfer process in acidic condition.

Data availability

The authors declare that all data supporting the findings of this study are available within the paper and Supplementary Information files. Source data are provided with this paper.

References

1. Yang, Y. et al. Engineering β-ketoamine covalent organic frameworks for photocatalytic overall water splitting. *Nat. Commun.* **14**, 593 (2023).
2. Ezendam, S. et al. Hybrid plasmonic nanomaterials for hydrogen generation and carbon dioxide reduction. *ACS Energy Lett.* **7**, 778–815 (2022).
3. Takata, T. et al. Photocatalytic water splitting with a quantum efficiency of almost unity. *Nature* **581**, 411–414 (2020).
4. Yoshino, S., Takayama, T., Yamaguchi, Y., Iwase, A. & Kudo, A. CO_2 reduction using water as an electron donor over heterogeneous photocatalysts aiming at artificial photosynthesis. *Acc. Chem. Res.* **55**, 966–977 (2022).
5. Rahman, M. Z., Raziq, F., Zhang, H. & Gascon, J. Key strategies for enhancing H_2 production in transition metal oxide based photocatalysts. *Angew. Chem. Int. Ed.* **62**, e202305385 (2023).
6. Dong, B., Cui, J., Qi, Y. & Zhang, F. Nanostructure engineering and modulation of (oxy)nitrides for application in visible-light-driven water splitting. *Adv. Mater.* **33**, 2004697 (2021).
7. Xiao, J., Hisatomi, T. & Domen, K. Narrow-band-gap particulate photocatalysts for one-step-excitation overall water splitting. *Acc. Chem. Res* **56**, 878–888 (2023).
8. Kataoka, Y. et al. Photocatalytic hydrogen production from water using porous material [Ru2(p-BDC)2]n. *Energy Environ. Sci.* **2**, 397–400 (2009).
9. Navalón, S., Dhakshinamoorthy, A., Álvaro, M., Ferrer, B. & García, H. Metal-organic frameworks as photocatalysts for solar-driven overall water splitting. *Chem. Rev.* **123**, 445–490 (2023).
10. Wang, X. et al. A metal-free polymeric photocatalyst for hydrogen production from water under visible light. *Nat. Mater.* **8**, 76–80 (2009).
11. Jin, E. et al. 2D sp^2 carbon-conjugated covalent organic frameworks for photocatalytic hydrogen production from water. *Chem* **5**, 1632–1647 (2019).
12. Banerjee, T., Podjaski, F., Kröger, J., Biswal, B. P. & Lotsch, B. V. Polymer photocatalysts for solar-to-chemical energy conversion. *Nat. Rev. Mater.* **6**, 168–190 (2021).
13. Ran, J., Zhang, J., Yu, J., Jaroniec, M. & Qiao, S. Earth-abundant cocatalysts for semiconductor-based photocatalytic water splitting. *Chem. Soc. Rev.* **43**, 7787–7812 (2014).
14. Li, Y. et al. In situ photodeposition of platinum clusters on a covalent organic framework for photocatalytic hydrogen production. *Nat. Commun.* **13**, 1355 (2022).
15. Yu, X., Zhao, H., Hu, J. & Chen, Z. Homojunction for biomass photorefinery. *Chem. Eng. J.* **498**, 155180 (2024).
16. Chen, R. et al. Spatiotemporal imaging of charge transfer in photocatalyst particles. *Nature* **610**, 296–301 (2022).
17. Sachs, M. et al. Tracking charge transfer to residual metal clusters in conjugated polymers for photocatalytic hydrogen evolution. *J. Am. Chem. Soc.* **142**, 14574–14587 (2020).
18. Moniz, S. J. A., Shevlin, S. A., Martin, D. J., Guo, Z.-X. & Tang, J. Visible-light driven heterojunction photocatalysts for water splitting - a critical review. *Energy Environ. Sci.* **8**, 731–759 (2015).
19. Nikoloudakis, E. et al. Porphyrins and phthalocyanines as biomimetic tools for photocatalytic H_2 production and CO_2 reduction. *Chem. Soc. Rev.* **51**, 6965–7045 (2022).
20. Lin, C. et al. Rational modification of two-dimensional donor-acceptor covalent organic frameworks for enhanced visible light photocatalytic activity. *ACS Appl. Mater. Interfaces* **13**, 27041–27048 (2021).
21. Chen, Y. et al. Bandgap engineering of covalent organic frameworks for boosting photocatalytic hydrogen evolution from water. *J. Mater. Chem. A* **10**, 24620–24627 (2022).
22. Kandambeth, S. et al. Construction of crystalline 2D covalent organic frameworks with remarkable chemical (acid/base) stability via a combined reversible and irreversible route. *J. Am. Chem. Soc.* **134**, 19524–19527 (2012).

23. Wang, H. et al. Integrating suitable linkage of covalent organic frameworks into covalently bridged inorganic/organic hybrids toward efficient photocatalysis. *J. Am. Chem. Soc.* **142**, 4862–4871 (2020).
24. Xiao, Y. et al. Visible-light-responsive 2D cadmium-organic framework single crystals with dual functions of water reduction and oxidation. *Adv. Mater.* **30**, 1803401 (2018).
25. Wu, S. et al. The keto-switched photocatalysis of reconstructed covalent organic frameworks for efficient hydrogen evolution. *Angew. Chem. Int. Ed.* **62**, e202309026 (2023).
26. Mathew, K., Kolluru, V. S. C., Mula, S., Steinmann, S. N. & Hennig, R. G. Implicit self-consistent electrolyte model in plane-wave density-functional theory. *J. Chem. Phys.* **151**, 234101 (2019).
27. Garcia-Ratés, M. & López, N. Multigrid-based methodology for implicit solvation models in periodic DFT. *J. Chem. Theory Comput.* **12**, 1331–1341 (2016).

Acknowledgements

This work was supported by the National Natural Science Foundation of China (22479040, 22002033, 21925206, 22332005, 22471055); the Natural Science Foundation of Hebei Province (B2022202049, B2022202039); Young Scientific and Technological Talents (Level Three) in Tianjin (QN20230343); Hebei Yanzhao Golden Platform Talent Gathering Plan Backbone Talent Project (HJYB202501).

Author contributions

F.Z. raised the design of materials. B.D. formulated and supervised the project. X.D. and H.J. performed the syntheses and analyses of COFs. Y.X., S.D., and Z.F. performed the DFT calculations. B.D. and X.D. wrote the manuscript. R.W. and F.Z. contributed to the data analysis, discussion, and manuscript revision.

Competing interests

The authors declare no competing interests.

Additional information

Supplementary information The online version contains supplementary material available at https://doi.org/10.1038/s41467-025-58337-w.

Correspondence and requests for materials should be addressed to Beibei Dong, Ruihu Wang or Fuxiang Zhang.

Peer review information *Nature Communications* thanks Reiner Sebastian Sprick who coiewed with Ewan McQueenand the other, anonymous, reviewers for their contribution to the peer review of this work. A peer review file is available.